J Mater Sci (2008) 43:12–22
DOI 10.1007/s10853-007-2150-4

Hydrogen embrittlement susceptibility of microstructures formed in multipass weld metal for HT780 class steel

Yoshihiko Kitagawa · Kenji Ikeuchi · Toshio Kuroda · Yukinobu Matsushita · Kazuyuki Suenaga · Takeshi Hidaka · Hideaki Takauchi

Received: 20 June 2007 / Accepted: 10 September 2007 / Published online: 8 November 2007

Abstract The effect of reheating by following passes on the hydrogen embrittlement of MAG weld metal for HT780 class steels has been investigated by using specimens subjected to simulated thermal cycles. The hydrogen-charged specimens exhibited transgranular quasi-cleavage fracture and intergranular fracture along prior austenite grain boundaries on slow strain rate tensile (SSRT) tests, depending on the reheated temperature and charged hydrogen content. The reduction in elongation of hydrogen-charged specimens became more significant when intergranular fracture occurred. When specimens in as-welded state and precedently reheated at coarse grained HAZ temperature of 1,623 K were reheated at a tempering temperature of 873 K, significant amount of intergranular fracture occurred at charged hydrogen contents above 3 ppm in spite of the decrease in hardness. The specimen reheated at 1,173 K showed no intergranular fracture even after receiving the reheating at 873 K at a hydrogen content of 6 ppm, suggesting the strong influence of the prior austenite grain size on the hydrogen-induced intergranular embrittlement. The measurement of hydrogen content desorbed from the hydrogen-charged specimen at room temperature suggested that the intergranular fracture caused by the reheating at 873 K was associated with an increase in susceptibility to hydrogen embrittlement of the prior austenite grain boundary itself rather than a decrease in the amounts of trapping sites such as dislocation and retained austenite.

Y. Kitagawa (✉) · K. Ikeuchi · T. Kuroda
Joining and Welding Research Institute, Osaka University, 11-1 Mihogaoka, Ibaraki, Osaka 567-0047, Japan
e-mail: kitagawa@jwri.osaka-u.ac.jp

Y. Matsushita · K. Suenaga · T. Hidaka · H. Takauchi
Kobe Steel, Ltd., 100-1, Miyamae, Fujisawa, Kanagawa 251-8551, Japan

Introduction

Recently, the susceptibility to hydrogen-induced cold cracking of the weld heat-affected zone (HAZ) of high strength steel has been significantly improved mainly by reducing the C and impurities contents [1]. This improvement made it possible to prevent the weld cold cracking of steels having tensile strengths lower than 590 MPa without preheating treatment. However, it is known that steels over 780 MPa class suffer from cold cracking occurring in the weld metal rather than the HAZ, when a preheating treatment is not given. Yatake et al. [2] and Okuda et al. [3] estimated the preheating and interpass temperature required to prevent the hydrogen-induced cold cracking in the weld metal of high strength steels of 690–980 MPa classes. They proposed that the preheating and interpass temperature was empirically given by the following equation:

$$T(^{\circ}\mathrm{C}) = A\sigma_{\mathrm{B}} + B\log[\mathrm{H}]_{\mathrm{D}} + Ch_{\mathrm{w}} + D, \quad (1)$$

where T is the preheating and interpass temperature, σ_{B} is the tensile strength of the weld metal, $[\mathrm{H}]_{\mathrm{D}}$ is the diffusible hydrogen content in the weld metal, h_{w} is the weld metal height, and A, B, C, and D are constants. Using Eq. 1, the preheating temperature necessary for the gas shielded metal arc weldments of 780 and 880 MPa class steels at the weld metal height of 20 mm are estimated to be 360–420 K and 440–500 K at hydrogen contents from 3 to 10 ppm, respectively [2]. It is said that the preheating treatment is a major factor limiting wider applications of high strength steels.

Many investigations were reported of the cold cracking in weld metal of high strength steels using single-pass [4–7] and multipass [2, 3, 8–10] weld tests. Important factors suggested in these investigations are the weld metal strength, diffusible hydrogen content, level of the residual stress, and the cooling rate. Hart [7] examined the influence of composition and microstructure on cold cracking resistance of weld metal using the gapped bead-on-plate (G-BOP) test. They reported that the effect of microstructure was dominant at hydrogen contents less than 5 mL/100 g, while the effect of hardness became dominant at higher hydrogen contents. Kim et al. [9] investigated the effects of microstructural and microhardness variations on the formation of hydrogen-induced cold cracks in the mutipass weld metal of HSLA-100 steel. They found that cold cracks initiated from the area having columnar grain structure that was tempered to some extent, and a localized increase in microhardness was not necessarily related to an increase in the susceptibility to cold cracking.

As suggested by these previous investigations, the microstructure may be considered to have a strong influence on the susceptibility to cold cracking in the weld metal of high strength steels. Conventional cold cracking tests employed in these investigations are useful to evaluate the hydrogen embrittlement susceptibility under conditions similar to those of real welding; however, it is not necessarily suitable to discuss the effect of individual factors such as microstructure, hydrogen content, and residual stress. Due to this, the hydrogen embrittlement susceptibilities of various microstructures that formed in the multipass weld metal do not seem to be thoroughly evaluated, and the understanding of microstructural factors responsible for the hydrogen embrittlement of the weld metal has not been well established.

The aim of the present investigation is to evaluate the hydrogen embrittlement susceptibility of various microstructures observed in a multipass weld metal for HT780 class steel, and to discuss microstructural factors controlling the hydrogen embrittlement of the multipass weld metal. For this, to obtain the weld metal microstructures formed by the reheating during following weld passes, specimens cut from a MAG weld metal of 780 MPa class steel were subjected to thermal cycles having various peak temperatures with a weld simulator, Gleeble 1500.

Experimental procedure

Base metal plates of 20 mm thickness were welded by MAG process in the shielding gas of Ar + 20% CO_2 using a welding wire designed for HT780 class steel (AWS A5.28 ER120S-G). To avoid the dilution of the weld metal with the base metal, the plate edges, which were beveled at an angle of 45°, were buttered with two layers of the weld metal. Then the groove was filled up with 12 weld beads in six layers. The weld heat input was 1.7 kJ/mm, and preheating and interpass temperatures were 423 K. The chemical composition of the deposited weld metal is shown in Table 1. Round-bar specimens $\phi 6 \times 70$ mm were machined parallel to the welding direction from the final weld bead to obtain the specimen of weld metal without a reheated area.

A thermal cycle simulating the reheating by a following pass was applied to the specimen using a resistance-heat weld simulator (Gleeble 1500). The peak temperatures of the simulated thermal cycles used were coarse grain HAZ temperature 1,623 K, fine grain HAZ temperature 1,173 K, intercritical temperature 973 K, and tempering temperature 873 K. The thermal cycle for the simulation was determined based on the measurement of the weld metal temperature with thermocouple during welding the final (12th) bead. Thermocouples were resistance-welded at the bottoms of holes that were drilled from the back surface of the plate to depths of 11.5–15 mm. The cooling times from 1,073 K to 773 K (Δt_{8-5}) were 17 s and 19 s for the thermal cycles with peak temperatures of 1,623 K and 1,173 K, respectively.

The as-welded and reheated specimens were machined to tensile specimens of gauge length 12 mm and diameter 3 mm. Hydrogen was introduced into the tensile test specimen by cathodic charging for 28.8 ks at a room temperature. The electrolytes for the cathodic charging were aqueous solutions of 1 N H_2SO_4 to which $NaAsO_2$ of 2, 10, and 250 mg/L was added. The current density for hydrogen charging was changed from 20 A/m^2 to 500 A/m^2, depending on the concentration of $NaAsO_2$. The charged hydrogen content could be varied from 1 ppm to 8 ppm in weight with an increase in $NaAsO_2$ content from 2 mg/L to 250 mg/L. As soon as hydrogen charging was finished, the specimen was electroplated with zinc in order to restrain the hydrogen desorption. The electroplating solution was composed of 350 g/L $ZnSO_4 \cdot 7H_2O$, 20 g/L H_2SO_4, 60 g/L Na_2SO_4, and distilled water. The

Table 1 Chemical composition of weld metal for HT780 class steel (elemental weight %)

C	Si	Mn	P	S	Ni	Cr	Cu	Mo	Ti	Fe
0.06	0.4	1.2	0.003	0.002	3.4	0.02	0.2	0.8	0.04	Bal.

electroplating was carried out for about 0.24 ks at a current density of 5 kA/m^2 at 333 K.

The hydrogen-charged specimen was subjected to slow strain rate tensile (SSRT) tests immediately after zinc-electroplating. The test was carried out using a universal testing machine (Shimadzu AG-10TB) at a constant cross head speed of 5×10^{-3} mm/min (strain rate = 6.94×10^{-6}/s). The hydrogen embrittlement susceptibility was evaluated from the tensile strength and elongation.

The cross sectional microstructures of the bar specimen receiving the reheating thermal cycle were examined by optical microscopy and transmission electron microscopy (TEM). The microstructure for the optical microscopy was revealed by etching in a 3% Nital solution. The thin foil specimens for the TEM observation were prepared using a focused ion beam (FIB) instrument (Hitachi High-Technologies FB-2000A). The transmission electron microscope used in this study was a JEOL JEM-2010, operating at an acceleration voltage of 200 kV. Hardness measurements with a Vickers tester and measurements of retained-austenite content by the X-ray diffraction method were also carried out using the specimens prepared for optical microscopy.

Experimental results

Optical microstructures of the as-welded and reheated specimens are shown in Fig. 1. The as-welded microstructure (Fig. 1a) consisted mainly of fine lath structures with only small amounts of grain boundary ferrite. The martensitic microstructure was also observed which was characterized by featureless and darker islands surrounded by lath structures (indicated by arrows). The microstructure of the specimen reheated at 873 K (Fig. 1b) was similar to the as-welded microstructure, though the lath structure was slightly coarser and etched more deeply. The martensitic structure also showed darker contrasts. In the specimen reheated at 973 K (Fig. 1c), the lath structure was degraded and the amount of martensitic structure was increased. In the intercritical temperature range, the microstructure of the steel consists of ferrite of lower *C* content and austenite of higher *C* content. Since increase in *C* content enhances the hardenability of steel, it can be considered that the specimen reheated at 973 K involved the larger amount of martensitic structure, which was transformed from the austenite enriched in *C*. At a reheating temperature of 1,173 K (Fig. 1d), the microstructure became finest of all the reheating temperatures, and the lath structure was degraded. Relatively high amount of martensitic structure was observed among the degraded lath structure. The microstructure of the specimen reheated at 1,623 K (Fig. 1e) consisted of lath structures and small amounts of martensitic structure. The prior austenite grain and the lath structure became coarser than the as-welded specimen. Small amounts of bainitic structures nucleated at prior austenite grain boundaries were also observed (indicated by arrows).

It is well accepted that the hardness is a principal measure to evaluate the hydrogen embrittlement susceptibility of the weld HAZ of steel. In this study, therefore, the microhardness of the specimen was measured with a Vickers hardness tester. The load for indentation was 1.96 N, and more than five points were measured for each specimen to acquire the average value. The result is shown in Fig. 2. The specimen reheated at 973 K showed the highest hardness of

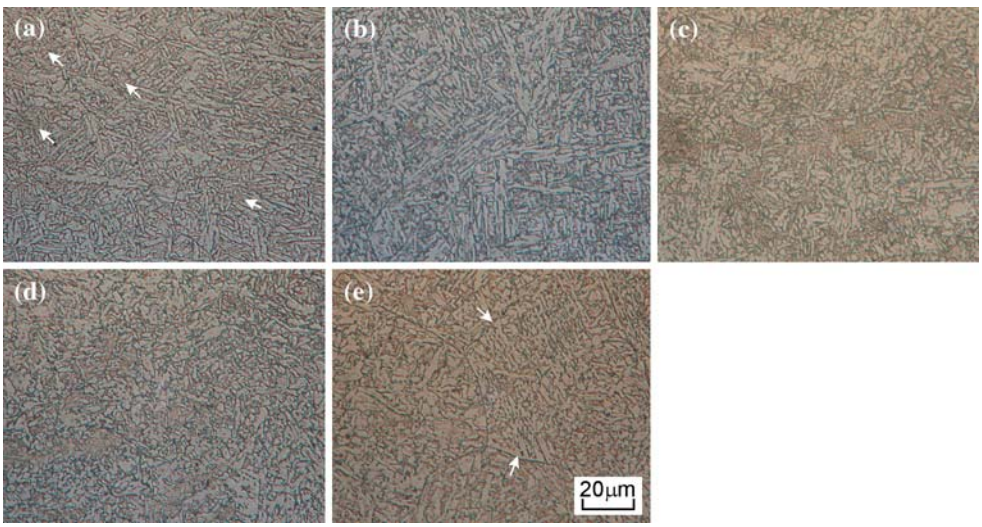

Fig. 1 Optical microstructures of the weld metal: (**a**) in as-welded state, (**b**) reheated at 873 K, (**c**) reheated at 973 K, (**d**) reheated at 1,173 K and (**e**) reheated at 1,623 K

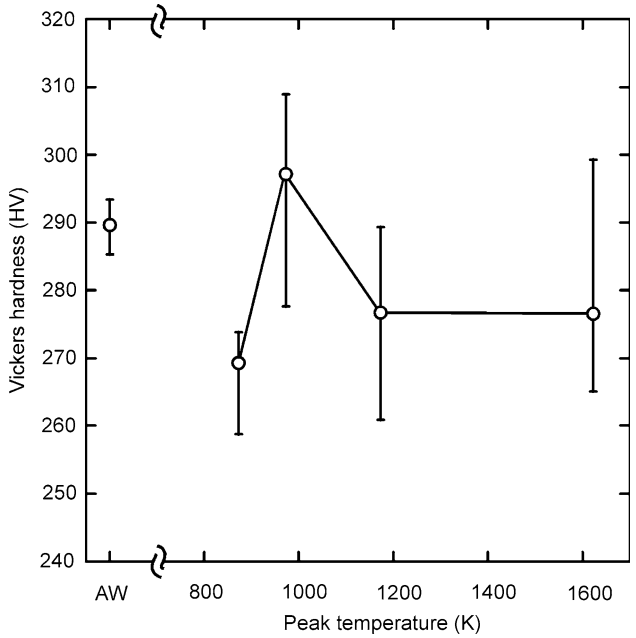

Fig. 2 Relation between reheating peak temperature and Vikers microhardness

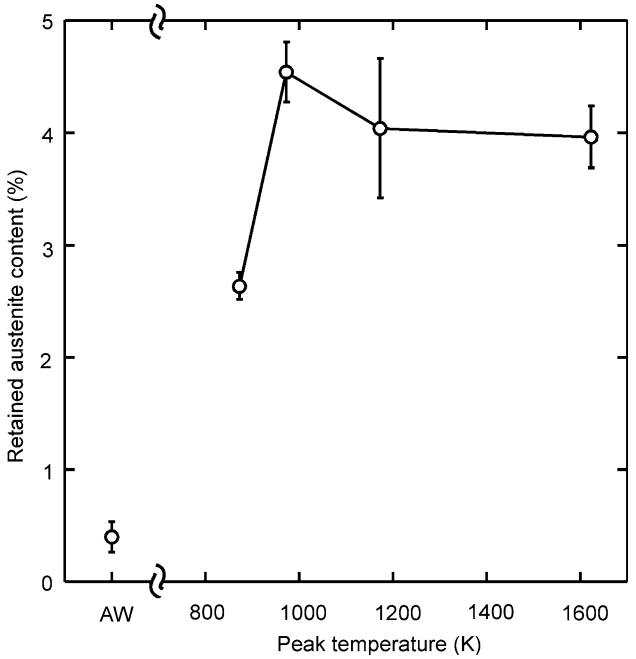

Fig. 3 Relation between reheating peak temperature and retained austenite content

300 HV. This corresponds to the result from the optical microscopy, which indicated that the amount of martensitic structure became highest at a reheating temperature of 973 K. The specimen reheated at 873 K showed the lowest hardness of 270 HV, probably owing to the tempering effect during the reheating. The hardness values of the specimens reheated at 1,173 K and 1,623 K were slightly lower than that of the as-welded specimen.

The content of retained austenite that could act as a trapping site of hydrogen [11] was evaluated based on X-ray diffractometry. The measurement was carried out using CuKα radiation with a diffractometer equipped with a graphite monochromator in the diffracted beam path. Diffraction peaks used for the measurement were 200, 211, and 220 for ferrite (involving martensite), and 200, 220, and 311 for austenite. The result is shown in Fig. 3. The retained austenite content was lowest in the as-welded specimen (0.4%), and it became highest when the specimen was reheated at 973 K (4.5%). The highest austenite content at a reheating temperature of 973 K can be attributed to the higher C content of the austenite that formed at reheating temperatures between Ac_1 and Ac_3 temperatures (α–γ coexisting temperature range), since C is an austenite-stabilizing element. The reason for the increase in retained austenite content of the tempered specimen (2.6%) in comparison with the as-welded specimen cannot be explained clearly. The solidification segregation of alloying elements lowering the Ac_1 temperature might be a possible mechanism to explain the increase in austenite content by reheating at 873 K. However, almost the same amount of austenite was detected even when a specimen was reheated at 873 K subsequently to reheating at 1,173–1,623 K as described later, though the solidification segregation mostly disappeared during the reheating at temperatures above Ac_3 point.

Stress–strain curves obtained from SSRT tests are shown in Fig. 4. As shown in Fig. 4a, the elongation and tensile strength of the as-welded specimen decreased significantly when 3 ppm hydrogen was introduced. The hydrogen-charged specimen showed two types of embrittled fracture morphologies (see Figs. 7 and 10): transgranular quasi-cleavage and intergranular fracture along prior austenite grain boundaries. The reduction in elongation was more serious when the specimen exhibited the intergranular fracture. When the specimen was reheated to 873 K and charged with 4 ppm hydrogen, the intergranular fracture was observed over significant areas of the fracture surfaces, and the tensile strength and elongation were remarkably degraded as shown in Fig. 4b. Thus, the intergranular fracture was observed in the as-welded and 873 K-reheated specimens at hydrogen contents not less than 3 ppm, while at hydrogen contents of 1 ppm or less, ductile fracture was dominant with only small areas of transgranular quasi-cleavage fracture (no intergranular fracture). As shown in Fig. 4c at a reheating temperature of 1,173 K, on the other hand, no specimen showed intergranular fracture, even though the hydrogen content was increased to 6 ppm. At this reheating temperature, the area of transgranular quasi-cleavage fracture of the specimen increased with the hydrogen content. The specimens

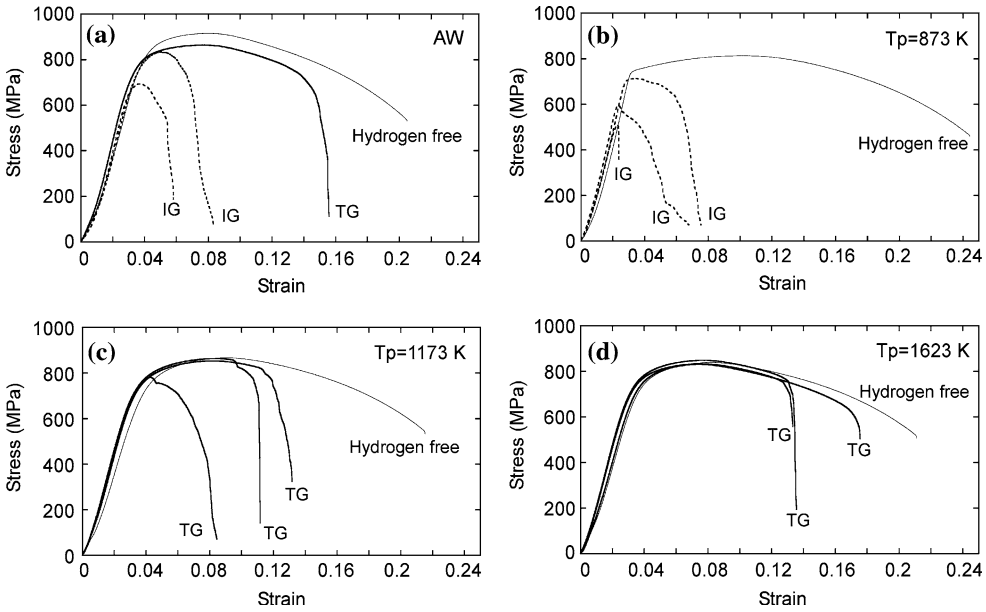

Fig. 4 Stress–strain curves during SSRT test where IG stands for intergranular fracture and TG stands for transgranular fracture: (**a**) as-welded specimens, (**b**) specimens reheated to 873 K, (**c**) specimens reheated to 1,173 K, and (**d**) specimens reheated at 1,623 K. Charged hydrogen contents of specimens in as-welded state was 3 ppm, and those of specimens reheated at 873 K, 1,173 K, and 1,623 K were 4 ppm, 6 ppm, and 6 ppm, respectively

reheated at 973 K and 1,623 K (Fig. 4d) showed similar behavior as the specimens reheated at 1,173 K except that one specimen reheated at 973 K fractured intergranularly when the hydrogen content was increased to 8 ppm.

The relation between charged hydrogen content and reduction in elongation is shown in Fig. 5. The reduction in elongation E_R (%) is given by $E_R = (E_0 - E)/E_0 \times 100$, where E_0 is the elongation of the specimen that was not subjected to the hydrogen charge and E is the elongation of hydrogen-charged specimen. When the specimens showed intergranular fracture (Fig. 5b), the reduction in elongation was remarkable, and it was more serious at a reheating temperature of 873 K than that observed in the as-welded state. The intergranular fracture became more dominant as the hydrogen content was increased, suggesting that it was caused by the charged hydrogen. When the specimens did not show intergranular fracture (Fig. 5a), the reduction in elongation was relatively small. In particular, at a reheating temperature of 873 K, the elongation of the specimen that showed no intergranular fracture was much greater than those of the other specimens.

In Fig. 6, the tensile strength is plotted against charged hydrogen content. The tensile strength of specimens that did not show intergranular fracture (Fig. 6a) was hardly affected by charged hydrogen content, since the fracture occurred at tensile loads near the maximum value. On the other hand, when the specimen showed intergranular fracture (Fig. 6b), the fracture occurred at stresses around the yield point where the stress changed largely with strain. For this, the increase in hydrogen content reduced considerably the tensile strength when the intergranular fracture occurred. The reduction in the tensile strength was noticeable when the reheating temperature was 873 K. From these results, it can be considered that the

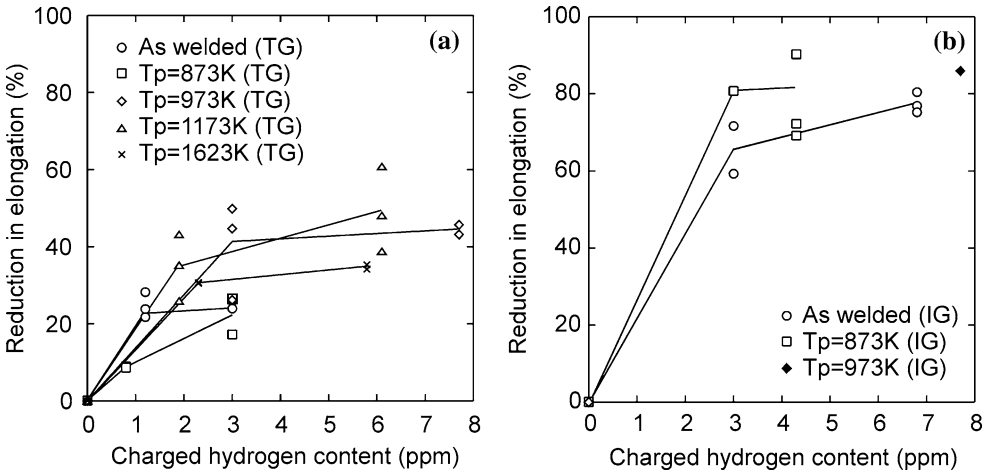

Fig. 5 Relation between charged hydrogen content and reduction in elongation for specimens, which did not show intergranular fracture (**a**) and for specimens which showed intergranular fracture (**b**). The reduction in elongation E_R is given by $E_R = (E_0 - E)/E_0 \times 100$, where E_0 is the elongation of specimen without hydrogen charging and E is the elongation of hydrogen-charged specimen

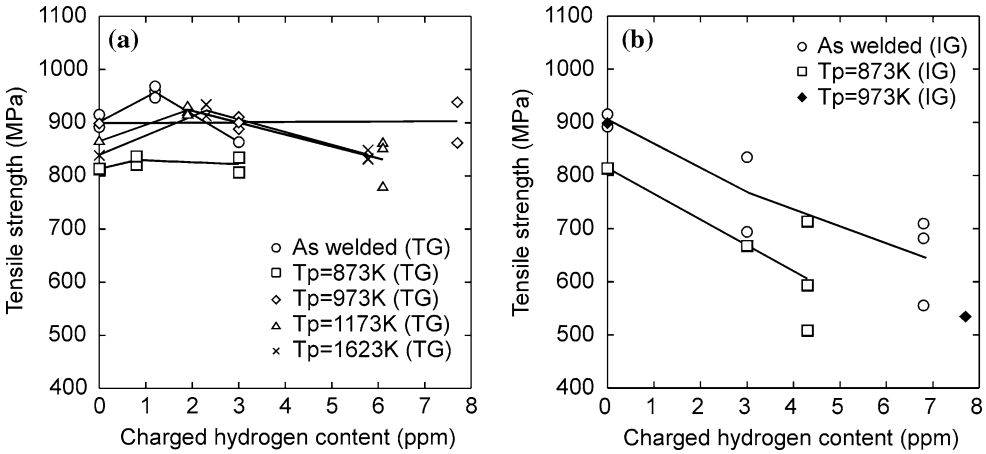

Fig. 6 Relation between charged hydrogen content and tensile strength for specimens, which did not show intergranular fracture (**a**) and for specimens which showed intergranular fracture (**b**)

specimen reheated at 873 K was most susceptible to the hydrogen embrittlement, though it had the lowest hardness of all the specimens investigated. This means that hardness is not a principal measure to evaluate the hydrogen embrittlement susceptibility of the weld metal for HT780 class steel.

The SEM micrographs of hydrogen-embrittled fracture surface of a specimen reheated at 873 K are shown in Fig. 7. The charged hydrogen content was 4 ppm. As shown in Fig. 7a, the specimen exhibited intergranular fracture surfaces along the boundary of columnar prior austenite grains and quasi-cleavage transgranular fracture surfaces among them. In the enlarged micrograph of the area of intergranular fracture (Fig. 7b), many small precipitates were observed, as indicated by arrows in the figure. These precipitates are considered to be carbides, judging from those observed by TEM microscopy (see Fig. 8). As shown in Fig. 7c, some carbides were observed to be accompanied with microvoids.

As-welded specimen in which 3 ppm hydrogen was introduced also showed intergranular fracture along columnar prior austenite grain boundaries in smaller areas (Fig. 9a). As shown in Fig. 9b, however, the amount of precipitates observed on the fracture surface were much less than that of the specimen reheated at 873 K, suggesting that the precipitates was not a principle factor for the intergranular fracture. As shown in Fig. 10, the specimen reheated at 1,173 K showed no intergranular fracture surface even when 6 ppm hydrogen was introduced, but transgranular quasi-cleavage fracture in significant areas.

In order to investigate the effect of the solidification segregation and prior austenite grain size on the occurrence of the intergranular fracture, the weld metal specimen was subjected to double reheating thermal cycles: the first cycle with peak temperatures of 1,173 K or 1,623 K, and the second one with a peak temperature of 873 K. When a specimen was reheated at 873 K subsequently to reheating at 1,173 K, as shown in Fig. 11a, the microstructure became slightly coarser and the martensitic structure showed darker contrasts than the specimen reheated only at 1,173 K. The retained austenite content of this specimen was estimated to be 2% as compared with 4% in the specimen reheated only at 1,173 K. The microstructure of the specimen reheated at 1,623 K was almost unaffected by the following reheating at 873 K except for slight coarsening of the lath structure as shown in Fig. 11b. The reheating treatment of 873 K decreased the retained austenite content of the specimen from 4% to 2.5%.

Stress–strain curves obtained from SSRT tests on these specimens are shown in Fig. 12. The reheating at 873 K increased considerably the elongation of the specimen reheated at 1,173 K when the hydrogen was not introduced (Fig. 12a). Even when the charged hydrogen content was 6.5 ppm, as shown in Fig. 12a, the specimen subjected to the double thermal cycles with a first reheating temperature of 1,173 K did not exhibit intergranular fracture as in the case where the second reheating at 873 K was not given. In addition, the reduction in elongation caused by hydrogen charging was significantly improved by the second reheating at 873 K. This result supports the conclusion that the reheating at a tempering temperature of 873 K lowers the susceptibility to transgranular quasi-cleavage fracture caused by hydrogen embrittlement. As shown in Fig. 12b, the reheating treatment of 873 K also improved the elongation of the specimen reheated at 1,623 K when hydrogen was not introduced. However, it brought about the intergranular fracture and serious impairment in the elongation when 4.5 ppm hydrogen was introduced. In contrast, as shown in Fig. 4d, no specimen reheated at 1,623 K showed intergranular fracture even at higher hydrogen contents, when the second reheating at 873 K was not given. A fracture surface of a specimen that was fractured intergranularly is shown in Fig. 13. As can be seen in this figure, the morphology of the fracture surface is the intergranular fracture along boundaries of equiaxed prior austenite grains, whereas those observed in the as-welded

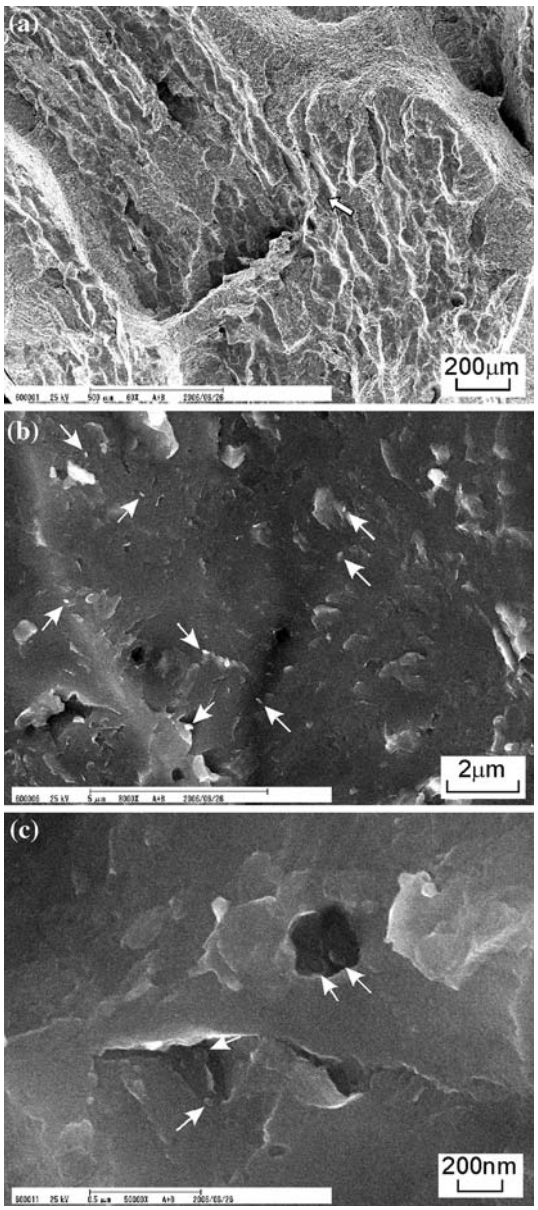

Fig. 7 Intergranular fracture surfaces of a specimen reheated at 873 K (charged hydrogen content ~4 ppm): (**a**) low magnification fractograph, (**b**) enlarged view of the area indicated by the arrow in (**a**), and (**c**) magnification of microvoids observed on the fracture surface

specimen presented a columnar structure after the reheating at 873 K. The elongation and tensile strength of hydrogen-charged specimens were comparable to or lower than that of the as-welded specimen subjected to reheating at 873 K.

Discussion

As described in the previous chapter, serious hydrogen-embrittlement due to the intergranular fracture along prior austenite grain boundaries occurred when the reheating treatment of 873 K was applied to specimens both in as-welded state and precedently reheated at 1,623 K. The fracture modes of a hydrogen embrittled specimen are generally discussed on the basis of the size of plastic zone ahead of a crack tip [12]; the plastic zone of large or medium size leads to dimple or transgranular quasi-cleavage fracture owing to the hydrogen trapped by the plastic zone, where microvoids or quasi-cleavage crack initiates due to the hydrogen accumulation; on the other hand, small plastic zone tends to induce the intergranular fracture since more hydrogen atoms are concentrated at grain boundaries without being trapped by the plastic zone. This is a mechanism believed by many authors to explain that the intergranular fracture becomes more dominant than the transgranular quasi-cleavage fracture as the tensile strength is increased in the hydrogen-induced embrittlement of high strength steels. However, this cannot account for our experimental results since specimens showing remarkable intergranular fracture had relatively low yield and tensile strengths as can be seen in Figs. 4 and 12.

With respect to the solidification segregation, the reheating at 873 K brought about the hydrogen-induced intergranular embrittlement whether the prior austenite grain was columnar (in as-welded state specimen) or equiaxed (in specimen reheated at 1,623 K). This suggests that the solidification segregation does not play an important role in the hydrogen-induced intergranular fracture, since the equiaxed austenite grain formed through $\alpha \rightarrow \gamma$ transformation during the reheating to 1,623 K, which removed the solidification microstructure.

Microstructural changes observed after the reheating at 873 K were (i) reduction in hardness, (ii) change in retained austenite content, (iii) increase in carbide precipitation, and (iv) slight coarsening of microstructure. A considerable part of the reduction in hardness can probably be ascribed to the decrease in dislocation density. The dislocation is known to decrease the apparent hydrogen mobility [13, 14] as a weak trapping site of hydrogen [15, 16]. Yang et al. [17] measured the dislocation density of acicular ferrite of welds containing 0.03 wt % carbon by transmission electron microscopy, and estimated it to be $(4 \pm 2) \times 10^{14}$ m^{-2}. Assuming that the number density of trap site of dislocation is 10^{10} m^{-1}, the number of trap sites accompanied by the dislocation of this density is $(4 \pm 2) \times 10^{24}$ m^{-3}, which corresponds to a hydrogen content of 0.8 ± 0.4 ppm if every site is occupied by a hydrogen atom. Morito et al. [18] measured the dislocation density of lath martensite of the steel containing 0.18 wt % C. The measured value ranged from 9×10^{14} m^{-2} to 13×10^{14} m^{-2}, which could trap 2–3 ppm hydrogen at maximum.

The retained austenite can also be considered to act as an effective trapping site because of the higher solubility of hydrogen than ferrite [19] and the slower hydrogen

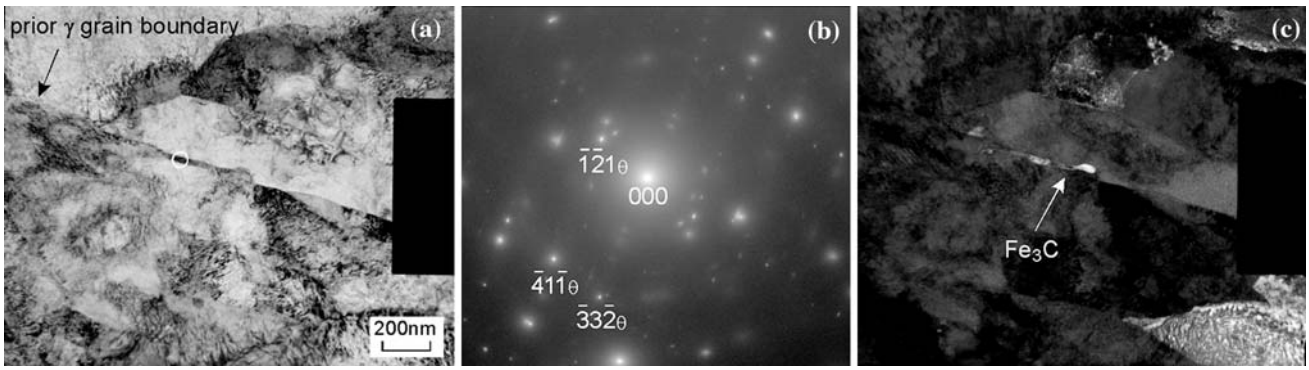

Fig. 8 TEM micrographs of a weld metal reheated at 873 K: (**a**) bright field image around prior austenite grain boundary, (**b**) SAD pattern from the area indicated by the circle in (**a**) (letter 'θ' indicates the reflection from Fe_3C, incident beam $\parallel [1\bar{5}\bar{9}]_\theta$), and (**c**) dark field image taken with $\bar{1}\bar{2}1_\theta$ diffraction beam

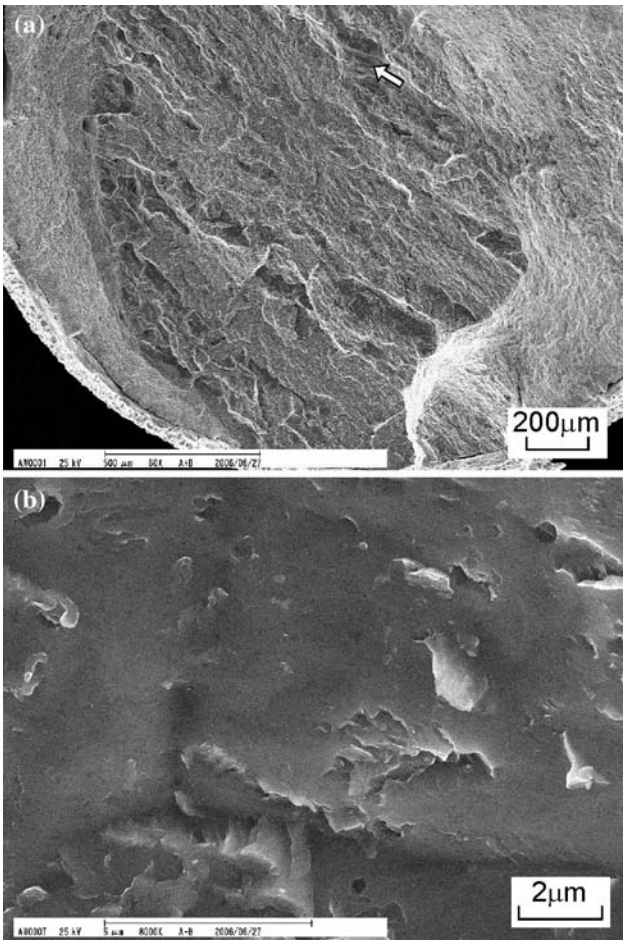

Fig. 9 Intergranluar fracture surface of an as-welded specimen (charged hydrogen content ~3 ppm): (**a**) low magnification fractograph and (**b**) enlarged view of the area indicated by the arrow in (**a**)

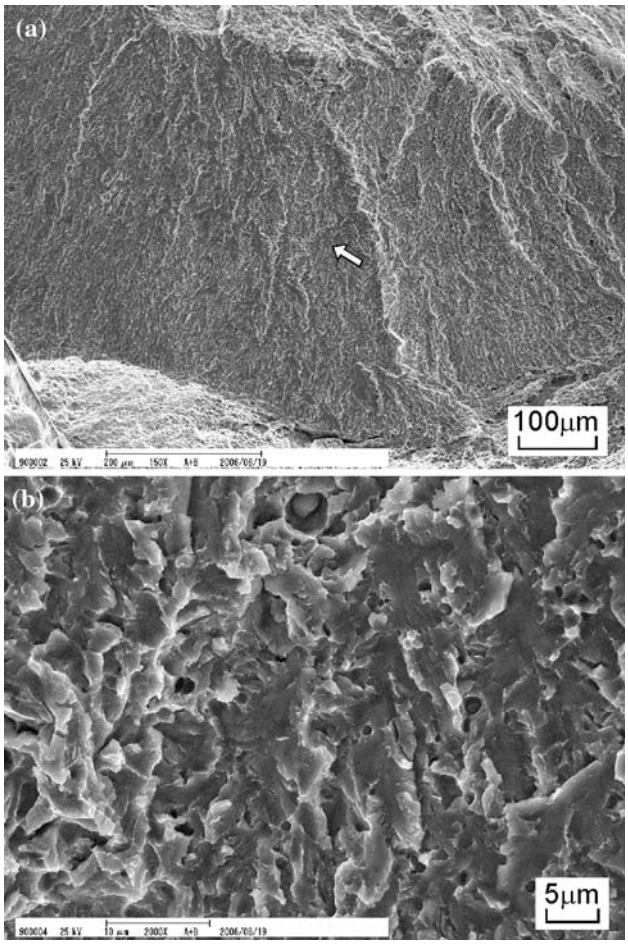

Fig. 10 Transgranluar quasi-cleavage fracture surface of a specimen reheated at 1,173 K (charged hydrogen content ~6 ppm): (**a**) low magnification fractograph and (**b**) enlarged view of the area indicated by the arrow in (**a**)

mobility [20, 21]. The distribution of hydrogen to ferrite and retained austenite can be expressed by the following equation:

$$V_\alpha C_\alpha + V_\gamma C_\gamma = C_T, \quad (2)$$

where V_α is a volume fraction of ferrite, V_γ is a volume fraction of retained austenite, C_α is a hydrogen content of ferrite, C_γ is a hydrogen content of retained austenite, and

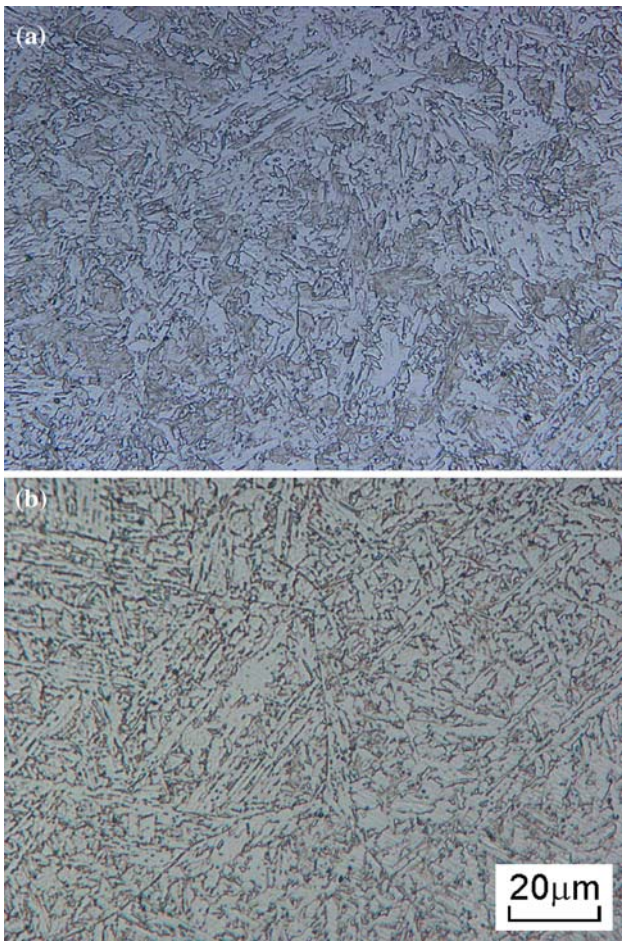

Fig. 11 Optical microstructures of the specimens reheated at 873 K subsequently to reheating at (**a**) 1,173 K and (**b**) 1,623 K

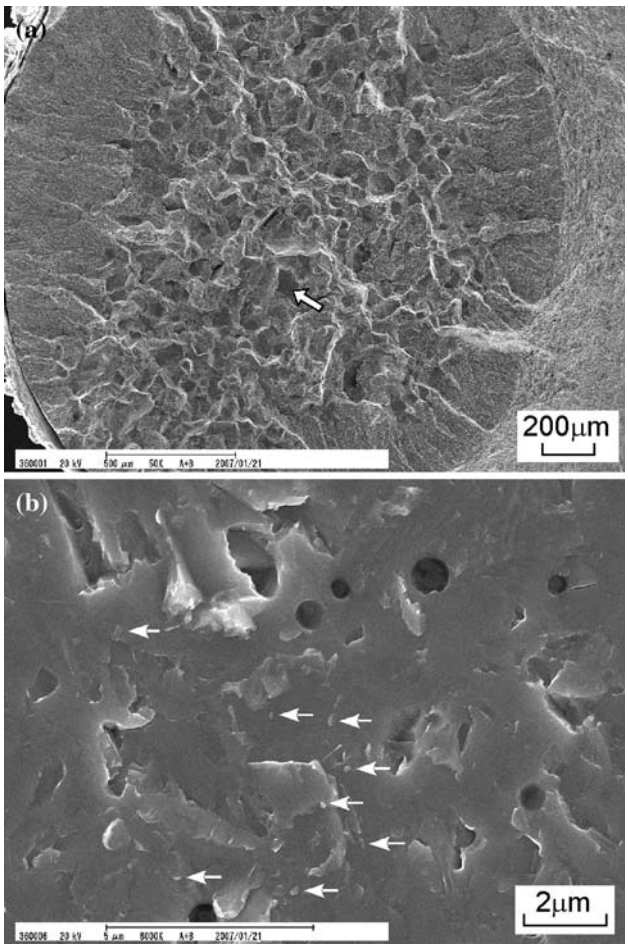

Fig. 13 Intergranluar fracture surface of the specimen reheated at 873 K subsequently to reheating at 1,623 K (charged hydrogen content was ~4.5 ppm): (**a**) low magnification fractograph and (**b**) enlarged view of the area indicated by the arrow in (**a**)

C_T is a total hydrogen content. Since $C_\alpha/C_\gamma < 1$ at room temperature [19], the hydrogen content of ferrite decreased with an increase in the volume fraction of retained austenite for a given total hydrogen content C_T.

It can be considered, however, that most of the trapping site in the hydrogen-charged specimen was occupied by hydrogen atoms since the charged hydrogen content was well above the solubility of the austenite as well as that of ferrite. In order to evaluate the content of mobile hydrogen at room temperatures, the amount of hydrogen desorbed from the specimen after hydrogen charging was measured based on gas chromatography. The specimens were hydrogen-charged under the same condition: at a current density of 100 A/m^2 for a charging time of 28.8 ks in 1 N H_2SO_4 + 10 mg/L $NaAsO_2$ solution. Although the experimental error was quite large (±1 ppm), as shown in Fig. 14, the amount of desorbed hydrogen of the specimen reheated at 873 K was smaller than those reheated at 973 K or 1,173 K. This suggests that amount of mobile hydrogen was smaller in the specimen reheated at 873 K than those

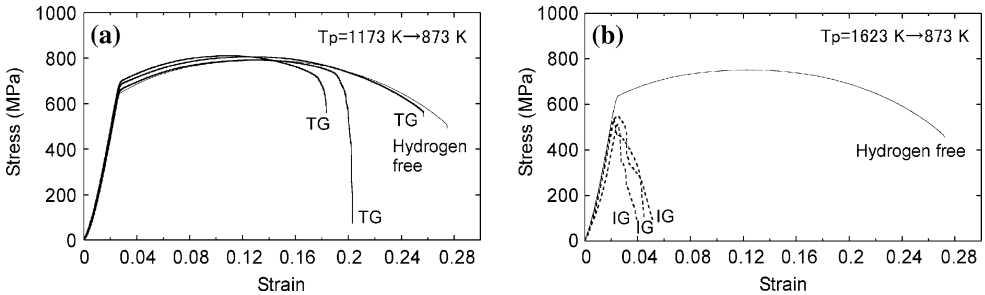

Fig. 12 Stress–strain curves during SSRT test of the specimens reheated at 873 K subsequently to reheating (**a**) at 1,173 K and (**b**) at 1,623 K. Charged hydrogen contents of the specimens precedently reheated at 1,173 K and 1,623 K were 6.5 ppm and 4.5 ppm, respectively

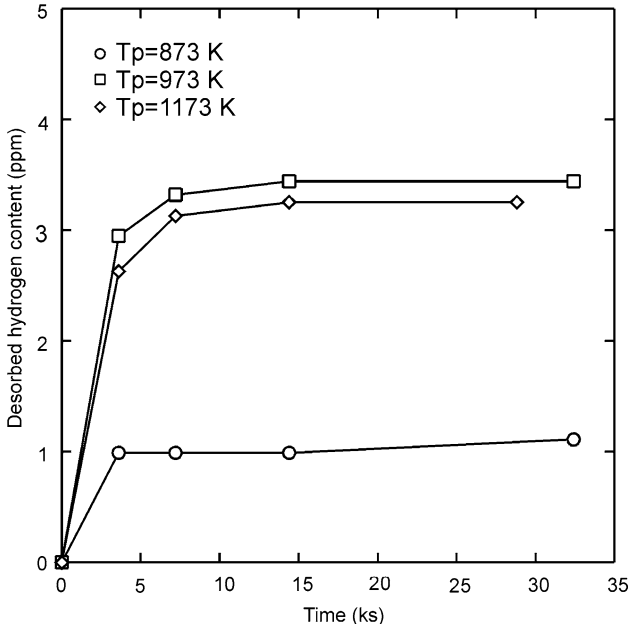

Fig. 14 Relation between desorbed hydrogen content and time after hydrogen charging for the specimens reheated at 873 K, 973 K, and 1,173 K

reheated at 973 K or 1,173 K, though the number of trap sites due to dislocations and retained austenite was decreased in the specimen reheated at 873 K. Therefore, it seems unlikely that the increase in the mobile hydrogen content due to the decrease in dislocation density and retained austenite volume causes the hydrogen-induced intergranular fracture observed in the specimen reheated at 873 K. In other words, the hydrogen-induced intergranular fracture observed in the specimen reheated at 873 K is attributable to the raised susceptibility to hydrogen embrittlement of prior austenite grain boundaries.

The carbide precipitation can be a factor increasing the hydrogen embrittlement susceptibility by trapping hydrogen atoms at the interface with matrix and serving as an initiation site of crack or microvoid. It was reported that hydrogen-induced microcrack initiated at the boundaries of carbide particles [22, 23] or film-like carbides [24]. Although the carbides observed in these investigations were much coarser (a few μm in size) than those observed in the present investigation (see Fig. 8), as shown in Fig. 7c, microvoids involving precipitates like carbides were observed on the intergranular fracture surface. Another possible effect of grain boundary carbides is to cause stress concentration at grain boundaries. The stress concentration encourages hydrogen build-up at grain boundaries under the tensile load. We have confirmed that no hydrogen embrittlement occurred when the tensile test was carried out at a faster strain rate (1.39×10^{-3}/s). This result suggests that the hydrogen was accumulated at grain boundaries through stress-induced diffusion during the SSRT test and the hydrogen accumulation through the stress-induced diffusion played an essential role in the intergranular fracture. In particular, if the carbide is precipitated preferentially at grain boundaries, it will raise greatly the susceptibility to intergranular fracture due to hydrogen embrittlement. From these points of view, the carbide precipitation at grain boundaries seems most responsible for the intergranular fracture of microstructural changes caused by reheating at 873 K. However, further investigations are necessary to understand the contribution of carbides to the intergranular fracture due to the hydrogen embrittlement.

It is known that tramp elements such as S and P segregated at grain boundaries at tempering temperatures and caused intergranular embrittlement of the high strength steel [25]. It is also accepted that the susceptibility to intergranular fracture due to hydrogen embrittlement is raised by the segregation [26–28]. However, the tempering time of the specimen reheated at 873 K is much shorter than those for which intergranular embrittlement was observed in the previous papers. Therefore, it is unconceivable that the significant grain boundary segregation of tramp elements was brought about by the reheating at 873 K.

The specimen reheated at 1,173 K (fine grained HAZ temperature) showed high resistance to intergranular fracture even after receiving subsequent reheating at 873 K, suggesting that prior austenite grain size had a strong influence on the hydrogen-induced intergranular embrittlement observed in the weld metal for HT780 class steel. There are some reports concerning the favorable effect of the refinement of prior austenite grain size on the resistance to intergranular fracture [29–31]. The possible factors to explain the effect of the grain refinement were (i) reduction in the dislocation accumulation at grain boundaries, (ii) decrease in hydrogen diffusivity due to grain refining [29], and (iii) decrease in effective grain size due to the refinement of intragranular microstructure [31]. As shown in Fig. 12b, the intergranular fracture occurred at stresses lower than the yield strength; i.e., fracture occurred before the dislocations accumulated significantly at grain boundaries. This suggests that factor (i) cannot account for the effect of grain refinement on the intergranular fracture observed in the present investigation. Hydrogen diffusivity, i.e., the content of mobile hydrogen is not considered to be a primary factor responsible for the low susceptibility to intergranular fracture of the specimen reheated at 1,173 K as suggested by the result shown in Fig. 14. Refinement of intragranular microstructure might be a factor enhancing the resistance to intergranular fracture by reducing the hydrogen concentration at prior austenite grain boundaries, since as shown in Fig. 1, the intragranular microstructure

observed after reheating at 1,173 K was quite different from those observed in as-welded and 1,623 K-reheated specimens.

Conclusions

1. As a result of SSRT test, two types of fracture morphology were observed in the hydrogen-charged specimen: transgranular quasi-cleavage fracture and intergranular fracture along prior austenite grain boundaries. The reduction in elongation due to the hydrogen charging was more remarkable, when the intergranular fracture occurred.
2. The intergranular fracture along prior austenite grain boundaries was observed in the as-welded specimen, the specimen reheated at 873 K, and the specimen subjected to the double heat treatments consisting of reheating cycles at 1,623 K and 873 K. The intergranular fracture became more dominant as the hydrogen content was increased. The specimen reheated at 1,173 K showed highest resistance to the intergranular fracture even after receiving the reheating at 873 K, suggesting the strong influence of the prior austenite grain size on the hydrogen-induced intergranular embrittlement.
3. It was found that the reheating at 873 K raised the susceptibility to the hydrogen-induced intergranular fracture and lowered the susceptibility to the transgranular quasi-cleavage fracture. The mechanism of intergranular fracture can be associated with the increase in susceptibility to hydrogen embrittlement of prior austenite grain boundaries rather than the decrease in the amounts of trapping sites such as dislocation and retained austenite.

References

1. Cullison A (1994) Weld J 73:51
2. Yatake T, Yurioka N, Kataoka R, Tsunetomi E (1981) J Jpn Weld Soc 50:291
3. Okuda N, Ogata Y, Nishikawa Y, Aoki T, Goto A, Abe T (1987) Weld J 66:141-s
4. Watkinson F (1969) Weld J 48:417-s
5. McParlan M, Graville BA (1976) Weld J 55:95-s
6. Alcantara NG, Rogerson JH (1984) Weld J 63:116-s
7. Hart PHM (1986) Weld J 65:14-s
8. Takahashi E, Iwai K (1979) J Jpn Weld Soc 48:865
9. Kim HJ, Kang BY (2003) ISIJ Int 43:706
10. Nevasmaa P (2004) Int Inst Weld 48(5/6):2
11. Park YD, Maroef IS, Landau A, Olson DL (2002) Weld J 81:27-s
12. Beachem CD (1972) Metall Trans 3:437
13. Kiuchi K, McLellan RB (1983) Acta Metall 31:961
14. Huang Y, Nakajima A, Nishikata A, Tsuru T (2003) ISIJ Int 43:548
15. Choo WY, Lee JY (1982) Metall Trans 13A:135
16. Wei FG, Tsuzaki K (2005) Scripta Mater 52:467
17. Yang JR, Bhadeshia HKDH (1990) Weld J 69:305-s
18. Morito S, Nishikawa J, Maki T (2003) ISIJ Int 43:1475
19. Easterling K (1983) In: Introduction to the physical metallurgy of welding. Butterworths, Sevenoaks, p 12
20. Perng TP, Altstetter CJ (1986) Acta Metall 34:1171
21. Chan SLI, Lee HL, Yang JR (1991) Metall Trans 22A:2579
22. Ju CP, Don J, Rigsbee JM (1986) Mater Sci Eng 77:115
23. Ju CP, Rigsbee JM (1988) Mat Sci Eng A 102:281
24. Krauss G, McMahon CJ Jr (1992) In: Olson GB, Owen WS (eds) Martensite. ASM International, New York, p 295
25. Mulford RA, McMahon CJ Jr, Pope DP, Feng HC (1976) Metall Trans 7A:1183
26. Yoshino K, McMahon CJ Jr (1974) Metall Trans 5:363
27. Briant CL, Feng HC, McMahon CJ Jr (1978) Metall Trans 9A:625
28. Murakami Y, Ohnishi K (1981) Bull Jpn Inst Metals 20:784
29. Lessar JF, Gerberich WW (1976) Metall Trans 7A:953
30. Kimura Y, Takagi S, Hara T, Terasaki S, Tsuzaki K (2003) J Phys IV 112:403
31. Kim HJ, Kim YH, Morris JW Jr (1998) ISIJ Int 38:1277